Briffa, A. K. R., Blackburn, E., Hayden, S. M., Yelland, E. A., Long, M. W., & Forgan, E. M. (2016). Fermi surface reconstruction and quantum oscillations in underdoped $YBa_2Cu_3O_{7-x}$ modeled in a single bilayer with mirror symmetry broken by charge density waves. *Physical Review B*, *93*, [094502]. https://doi.org/10.1103/PhysRevB.93.094502

Fermi surface reconstruction and quantum oscillations in underdoped $YBa_2Cu_3O_{7-x}$ modeled in a single bilayer with mirror symmetry broken by charge density waves

A. K. R. Briffa,[1,2] E. Blackburn,[1] S. M. Hayden,[3] E. A. Yelland,[4,5] M. W. Long,[1] and E. M. Forgan[1,*]

[1]*School of Physics and Astronomy, University of Birmingham, Birmingham B15 2TT, United Kingdom*

[2]*Crete Center for Quantum Complexity and Nanotechnology, University of Crete, Heraklion 71003, Greece*

[3]*H. H. Wills Physics Laboratory, University of Bristol, Bristol BS8 1TL, United Kingdom*

[4]*SUPA, School of Physics and Astronomy, University of St Andrews, St Andrews KY16 9SS, United Kingdom*

[5]*SUPA, School of Physics and Astronomy and CSEC, University of Edinburgh, Edinburgh EH9 3FD, United Kingdom*

(Received 9 October 2015; revised manuscript received 2 February 2016; published 1 March 2016)

Hole-doped high-temperature cuprate superconductors below optimum doping have electronlike Fermi surfaces occupying a small fraction of the Brillouin zone. There is strong evidence that this is linked to charge density wave (CDW) order, which reconstructs the large holelike Fermi surfaces predicted by band structure calculations. Recent experiments have revealed the structure of the two CDW components in the benchmark bilayer material $YBa_2Cu_3O_{7-x}$ in high field where quantum oscillation (QO) measurements are performed. We have combined these results with a tight-binding description of the bands in a single bilayer to give a minimal model revealing the essential physics of the situation. Here we show that this approach, combined with the effects of spin-orbit interactions and the pseudogap, gives a good qualitative description of the multiple frequencies seen in the QO observations in this material. Magnetic breakdown through weak CDW splitting of the bands will lead to a field dependence of the QO spectrum and to the observed fourfold symmetry of the results in tilted fields.

DOI: 10.1103/PhysRevB.93.094502

I. INTRODUCTION

In recent years, a clear picture of the variation of the electronic structure of cuprate high-T_c materials with doping has emerged. Overdoped materials have large holelike cylindrical Fermi surfaces with cross sections reflecting the single hole on a Cu^{2+} plus the additional carriers due to doping [1], whereas on the underdoped side of the superconducting dome, quantum oscillation (QO) measurements [2] indicate small electronlike Fermi surface (FS) areas that occupy only ∼2% of the Brillouin zone (BZ). This strongly suggested a FS reconstruction arising from broken translational symmetry [3]. Macroscopic measurements indicate a change to electronlike transport below ∼150 K in the underdoped region [4], which is consistent with the FS reconstruction scenario, and nuclear magnetic resonance (NMR) measurements [5] on underdoped $YBa_2Cu_3O_{7-x}$ (YBCO) give clear indications of charge density waves. The charge density wave (CDW) state has been seen by x-ray diffraction in YBCO [6–12]. It has been shown to be a ubiquitous high-T_c phenomenon [13–22], and there is strong evidence that the CDW order at high fields is intimately connected with the QO frequencies [17].

In zero magnetic field, the CDW displacements break the mirror symmetry of the CuO_2 bilayers [23]. In high magnetic fields, the CDW modulation along the crystal *b* direction of a YBCO sample develops long-range order [24]. The relationship of the high-field structure to the zero-field structure [23] has also been established [25] and it also breaks the mirror symmetry of the CuO_2 bilayers. Hence we now have the essential ingredients to give an explanation of the QO results. Unlike previous attempts, in our model we use the correct CDW symmetry, and choose our chemical potential to be consistent with the nodal FS recently seen by angle-resolved photoelectron spectroscopy (ARPES). We assume weak *c*-axis tunneling between bilayers in order to obtain the minimal model for the QO results. This approach reveals how much can be explained by a single-particle Fermi-liquid model, and raises some fascinating questions.

II. BASIC MECHANISM FOR THE FS RECONSTRUCTION

In the present paper, we consider the Fermi surface reconstruction of a single bilayer in which both **a** and **b** modulations are present in the same region of the sample. This coexistence is consistent with ultrasonic measurements on an underdoped YBCO sample [26] and the close-to-fourfold symmetry of the QO results [27]. Recent zero-field x-ray measurements [23] have shown that both of the CDWs exhibit a previously unsuspected symmetry breaking, and give opposite perturbations in the two halves of the superconducting CuO_2 bilayers. X-ray measurements also show [25] that this symmetry breaking is maintained at high magnetic fields $B \approx 17$ T, i.e., above the phase transition observed by ultrasound and NMR for fields $B \sim 15$–17 T. However, x-ray measurements [10,25] also indicate a very short *c*-axis correlation length for the CDW modulated along **a**, yet clear QO signals are observed in what is a somewhat disordered state. Thus we believe that it is reasonable to consider a single bilayer occasioned by weak *c*-axis tunneling between separate bilayers, which will be little affected by incomplete ordering along the *c* axis.

There is a hierarchy of electronic energy scales in this system, and we list the ones of relevance for this problem. The largest is the Coulomb energy, which ensures a Mott insulating state at zero doping. The next largest is the basal-plane hopping, which gives the shape and the Fermi velocity of the unreconstructed Fermi surface. There are then several effects which are of similar order of magnitude, and which we list in order of expected decreasing size: *c*-axis hopping between the two halves of a single CuO_2 bilayer, pseudogap energy (which we shall include only qualitatively), and the CDW perturbation. The energy of the carriers due to the applied magnetic

*Corresponding author: E.M.Forgan@bham.ac.uk

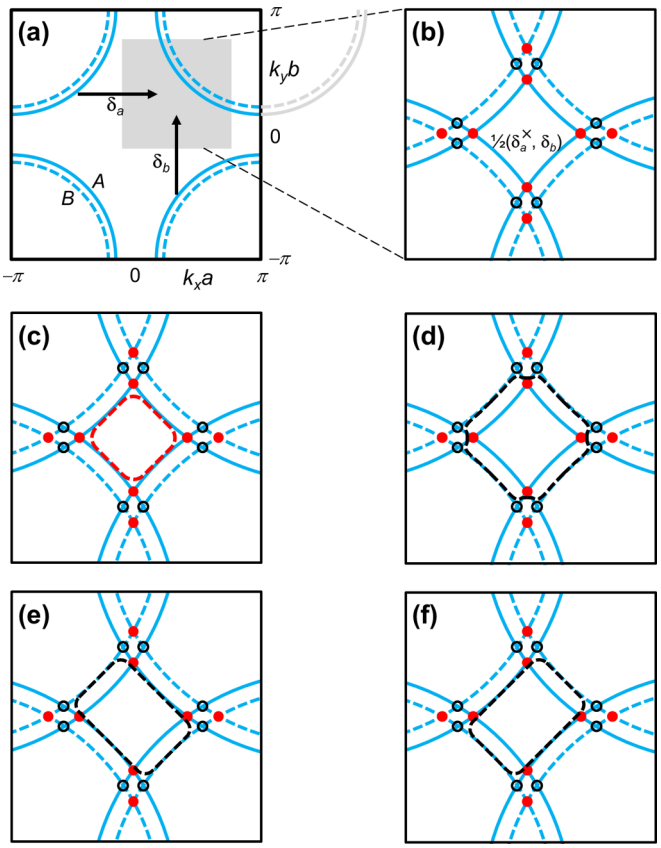

FIG. 1. Schematic illustration of CDW hybridization of CuO_2 bilayer electron states. In (a) are represented the FS sheets arising from the antibonding (A) and bonding (B, dashed line) bands of the CuO_2 bilayers in a $k_x - k_y$ cross section of the BZ for YBCO. These bands form *large* hole surfaces of approximately cylindrical shape around the corner of the BZ. The basal-plane parts of the CDW wave vectors $\boldsymbol{\delta}_a$ and $\boldsymbol{\delta}_b$ are shown approximately to scale. The shaded region in (a), which is centered on the point $\frac{1}{2}(\boldsymbol{\delta}_a, \boldsymbol{\delta}_b)$, is shown in the other five panels. The effects of the CDW components may be represented by translation of the bands in the other corners of the BZ by $\boldsymbol{\delta}_a$ and $\boldsymbol{\delta}_b$, giving crossings between states connected by one of the CDW wave vectors. The positions where the A and B states are degenerate and A-B hybridization may occur are marked with open black circles. At the red dots, there is A-A and B-B degeneracy, and weaker hybridization occurs. The resulting small electronlike FS pockets are shown in red and black. If the hybridization at the A-A crossings is weak, it can be crossed at high magnetic fields, and new FS areas, including those represented in (e) and (f), will result.

field must also be included: in a typical field of 50 T used in QO measurements, the Zeeman energy of the spins is $\sim\pm 3$ meV, and the splitting of the "orbital" Landau levels is similar. We expect that the spin-orbit interaction will be comparable in magnitude with this. Finally, we have the c-axis tunneling between separate bilayers, and we shall set this to zero in our model. We shall further discuss the values of the parameters in our model after investigating their relevance to the QO results.

In Fig. 1, we give a general outline of how the FS reconstruction arises from the CDW structures now established. The CDW perturbation can give strong hybridization between states at the same energy which are connected by the CDW $\mathbf{q}$ vectors. The relevant states may be visualized by translating Fermi surfaces by these $\mathbf{q}$ vectors into a corner of the BZ, as illustrated in Fig. 1. Because the CDW gives opposite perturbations in the two halves of a bilayer, the strongest hybridization takes place between the bonding (B) and antibonding (A) states of a bilayer, giving the avoided crossings at the points marked in black. However, spin-orbit effects discussed later can allow the CDW also to cause weaker hybridization at A-A and B-B crossings marked in red. This gives rise to two reconstructed FSs: the smaller one is of mainly A character and the larger is mainly constructed from the B bands. In high fields, the smaller gaps may be bridged by magnetic breakdown, giving several different FS areas, as observed in experiment. Parts of this general scenario have been invoked before [17,27–32], but none of these models used the correct form for the CDW perturbation, the hopping between the two halves of the bilayer, and the spin-orbit (SO) coupling at the FS crossing points. For optimally and underdoped cuprates, it is particularly clear that strong correlation effects, arising from the proximity to a Mott insulator state, are important. These are associated with the "pseudogap" (PG), which corresponds to the removal of states at the Fermi level, leaving "Fermi arcs" instead of complete Fermi surfaces. These have been observed in underdoped YBCO by photoemission (ARPES) [33]. The states removed by the PG are at the edges of Fig. 1 and do not participate in the formation of the small electronlike pockets. It is also found [33] that the states in the CuO chains are suppressed. QO observations in YBCO as a function of underdoping confirm this effect, as they give no indications of a chain FS (nor effects of chain ordering), and heat-capacity measurements at high field [34,35] also show that the chains are not metallic. These results indicate that first-principles density functional theory (DFT) calculations are not sufficiently accurate in the underdoped region, since they give a chain Fermi surface, and certainly do not give the PG.

Instead, to obtain tractable results, we carry out our calculations using a tight-binding approximation (TBA) for the band structure of a single CuO_2 bilayer, which can be used to give the shapes of the Fermi arcs, which are coupled by the CDW. This approach lays bare the essential physics because the symmetry of the band couplings caused by the CDW perturbations will be unaffected by the PG. In our two-dimensional model, we can ignore k_z, i.e., the c-axis component of the carrier wave vector, but our results can be extended [36] to take account of c-axis coherence revealed by transport measurements [37].

We first recount the properties of the bilayer states in the absence of a CDW. We then show how the hybridization of bilayer states by a CDW varies with their bonding or antibonding character, the bilayer coupling, and the presence of spin-orbit splitting. We use the results of DFT calculations to indicate general features of bilayer coupling in the TBA approach, and reveal some misconceptions in the literature about this. We show the results of our calculations for a set of parameters chosen to reveal the important features of the model that can give an account of features of the QO observations. We estimate the effects of magnetic breakdown across the CDW band gaps and show that this will be important. Finally, we discuss in general terms how this scenario can account for the experimental observations.

III. THE NATURE OF THE BILAYER WAVE FUNCTIONS AND EFFECTS ON CDW MATRIX ELEMENTS

Until now, it had been assumed that a CDW in YBCO would have even symmetry about the center of the bilayer and would only couple A to A and B to B bands [27,28]. However, structure determinations show that the CDW perturbation has odd symmetry, at both zero and high fields [23,25]. This perturbation may arise from CDW-associated changes in basal-plane hopping, local doping, or Coulomb potential, and all of these have opposite values in the two halves of a bilayer. In a single bilayer, the A and B states are usually assumed to have a definite parity so that the CDW perturbation couples only A to B. However, two effects negate this simple picture and allow weak hybridization by the CDW of A with A states and B with B. First, a Rashba-type spin-orbit interaction [38] gives an opposite energy shift to states of a given spin in the top and bottom layers. The importance of this interaction and the fact that it can flip carrier spin have recently been emphasized [31]. Second, if coupling between adjacent bilayers cannot be ignored, the A and B states do not have a definite parity at general k_z. Here we shall assume that this second effect can be neglected and consider this generalization in a further publication [36].

To set the scene, we sketch the TBA for the double Fermi surface sheets arising from the CuO_2 bilayer bands, ignoring the spin-orbit interaction for now. As described above, we also ignore the chain bands and, for simplicity, treat the YBCO cell as tetragonal with lattice parameters a and c. In the absence of bilayer coupling, the energy $\varepsilon(\mathbf{k})$ of a state relative to the Fermi energy ε_F in a single CuO_2 layer with basal-plane wave vector $\mathbf{k} = (k_x,k_y)$ is given by Ref. [39]:

$$\varepsilon(\mathbf{k}) = -2t(\cos k_x a + \cos k_y a) + 4t'(\cos k_x a \cos k_y a) - 2t''(\cos 2k_x a + \cos 2k_y a) - \varepsilon_F. \quad (1)$$

Typical ratios for the hopping matrix elements are $t' = 0.32t$ and $t'' = 0.16t$ [39], and the value of ε_F is chosen to give an almost half-filled BZ. This $\varepsilon(\mathbf{k})$ is then modified by the intrabilayer hopping $t_\perp$ and the coupling t_c of two adjacent bilayers in the c direction to give the two bilayer bands: bonding of lower energy and antibonding. We expect that $t_\perp$, t', t'', and also the CDW perturbation V will be of similar magnitude: in the region of 10 meV [10]. The bilayer energies and states in the absence of the CDW are given by a Hamiltonian matrix using the basis states on each half of a bilayer [40],

$$H_b(\mathbf{k},k_z) = \begin{bmatrix} \varepsilon(\mathbf{k}) & -t_\perp - t_c e^{-ik_z c} \\ -t_\perp - t_c e^{+ik_z c} & \varepsilon(\mathbf{k}) \end{bmatrix}. \quad (2)$$

The energy eigenvalues of this are

$$\varepsilon_{A,B}(\mathbf{k},k_z) = \varepsilon(\mathbf{k}) \pm \sqrt{t_\perp^2 + t_c^2 + 2t_\perp t_c \cos k_z c}. \quad (3)$$

Assuming that t_c is negligible, this reduces to $\varepsilon_{A,B}(\mathbf{k}) = \varepsilon(\mathbf{k}) \pm t_\perp$, where the $\pm$ ambiguity refers to the A and B bands, respectively. Note that the c-axis dispersion is removed if either of $t_\perp$ and t_c is zero, but the A-B splitting remains as long as at least one of them is nonzero.

We now introduce the spin-orbit (SO) interaction; there are several possible terms, but the important one for our purposes breaks the symmetry between the two halves of the bilayer for a state of given spin, and hence the hybridization by the CDW at crossings between bilayer states of *like* character becomes nonzero. The SO interaction arises because an individual CuO_2 layer does not have mirror symmetry in the z direction, so the states in each layer have a Rashba-type energy term [38]:

$$\delta_{\rm SO}(\mathbf{k}) = \alpha(\mathbf{k} \times \hat{\mathbf{z}}) \cdot \boldsymbol{\sigma} \rightarrow \alpha((\mathbf{k} - \mathbf{k}_{\rm corner}) \times \hat{\mathbf{z}}) \cdot \boldsymbol{\sigma}. \quad (4)$$

Here, $\boldsymbol{\sigma}$ is the spin operator and α gives the strength of this effect; in the original nearly free electron case [38], $\mathbf{k}$ would be proportional to the carrier momentum. For our purposes, a sufficiently good approximation is instead to take $\mathbf{k}$ relative to the nearest corner of the BZ, since the unreconstructed energy bands form approximately circular energy contours around these points. The sign of the term is opposite in the top and bottom layers. The Rashba term only involves σ_x and σ_y, which can be expressed in terms of eigenstates of σ_z using the Pauli spin matrices. We can write the Hamiltonian matrix including this term by using the layer states labeled by the z component of their spin, giving

$$H_{b+{\rm SO}}(\mathbf{k}) = \begin{bmatrix} \varepsilon(\mathbf{k}) + \mu B_z & \delta_{\rm SO}(\mathbf{k}) & -t_\perp & 0 \\ \delta_{\rm SO}^*(\mathbf{k}) & \varepsilon(\mathbf{k}) - \mu B_z & 0 & -t_\perp \\ -t_\perp & 0 & \varepsilon(\mathbf{k}) + \mu B_z & -\delta_{\rm SO}(\mathbf{k}) \\ 0 & -t_\perp & -\delta_{\rm SO}^*(\mathbf{k}) & \varepsilon(\mathbf{k}) - \mu B_z \end{bmatrix}. \quad (5)$$

Here, the first two basis states are in the upper half of the bilayer and have up and down spins with Zeeman energy $\pm\mu B_z$ in an applied field B_z; these states are coupled by the SO interaction. The other two basis states are in the lower half of the bilayer and have an SO interaction which is opposite in sign to that for the top layer. The (spin-independent) hopping terms connect states of the same spin in top and bottom layers, while the spin-orbit terms connect states of opposite spin in the same layer. In zero field, this Hamiltonian gives the A and B state energies, each of which is doubly (Kramers) degenerate due to the overall mirror symmetry of the bilayer,

$$\varepsilon_{A,B}(\mathbf{k}) = \varepsilon(\mathbf{k}) \pm \sqrt{t_\perp^2 + |\delta_{\rm SO}(\mathbf{k})|^2}. \quad (6)$$

Comparison with Eq. (3) shows that in the absence of a CDW, the spin-orbit term does not mix the A and B bands; it merely increases the A-B energy splitting. It does, however, give a weak admixture of spin up in the spin-down states, and vice versa. In nonzero field, there are four different eigenvalues, which for $|\delta_{\rm SO}(\mathbf{k})|$ and μB_z small compared with $t_\perp$ may be

labeled approximately as spin up and down in the A and B bands.

Finally, we introduce the CDW perturbation V. To first order, it only connects states in the same layer (and of the same spin) that differ by a single CDW $\mathbf{q}$ vector [27]. The antisymmetry of this perturbation means that its matrix element between basis states in the upper layer is equal and opposite to that for the lower half of the bilayer, and we may write the values as $\pm V$, respectively. Hence, to describe the hybridization between two sets of A and B bands, we have the 8×8 Hamiltonian matrix given in Eq. (7). (We refrain from reproducing the 16×16 matrix, which is the minimal model to represent all four crossings shown in Fig. 1.) In Eq. (7), the two 4×4 blocks on the diagonal reproduce Eq. (5) for the two sets of states connected by a CDW, while the off-diagonal blocks represent the CDW couplings between them. The basal-plane wave vector $\mathbf{k}' = \mathbf{k} \pm \boldsymbol{\delta}_a$ or $\pm\boldsymbol{\delta}_b$ for hybridization by an a- or b-direction CDW. For simplicity, we take the CDW matrix element V to have the same value for the a and b CDW modulations,

$$\begin{bmatrix}
\varepsilon(\mathbf{k})+\mu B_z & \delta_{\rm SO}(\mathbf{k}) & -t_\perp & 0 & V & 0 & 0 & 0 \\
\delta^*_{\rm SO}(\mathbf{k}) & \varepsilon(\mathbf{k})-\mu B_z & 0 & -t_\perp & 0 & V & 0 & 0 \\
-t_\perp & 0 & \varepsilon(\mathbf{k})+\mu B_z & -\delta_{\rm SO}(\mathbf{k}) & 0 & 0 & -V & 0 \\
0 & -t_\perp & -\delta^*_{\rm SO}(\mathbf{k}) & \varepsilon(\mathbf{k})-\mu B_z & 0 & 0 & 0 & -V \\
V & 0 & 0 & 0 & \varepsilon(\mathbf{k}')+\mu B_z & \delta_{\rm SO}(\mathbf{k}') & -t_\perp & 0 \\
0 & V & 0 & 0 & \delta^*_{\rm SO}(\mathbf{k}') & \varepsilon(\mathbf{k}')-\mu B_z & 0 & -t_\perp \\
0 & 0 & -V & 0 & -t_\perp & 0 & \varepsilon(\mathbf{k}')+\mu B_z & -\delta_{\rm SO}(\mathbf{k}') \\
0 & 0 & 0 & -V & 0 & -t_\perp & -\delta^*_{\rm SO}(\mathbf{k}') & \varepsilon(\mathbf{k}')-\mu B_z
\end{bmatrix}. \quad (7)$$

IV. *c*-AXIS COUPLING

The quantity $t_\perp$ arises from hopping between the two halves of a bilayer. It has been stated, e.g., in Refs. [28,31,39,40], that $t_\perp$ has a strong dependence on $\mathbf{k}$ and is zero on the nodal line $k_x = k_y$, but this is not the case. If $t_\perp$ were indeed zero at the nodal line, Eq. (3) indicates that there would be zero k_z dispersion on this line, whereas DFT calculations [39,41,42] show a nonzero dispersion. In adducing evidence from DFT calculations, we do not rely on their absolute accuracy, merely that if they give finite k_z dispersion, then they show that zero dispersion is *not* imposed by crystal symmetry. The origin of the supposed zero of $t_\perp$ is the assumption that the hopping between the two halves of the bilayer takes place at the Cu ions, via orbitals of s (or, equivalently, $d_{3z^2-r^2}$) symmetry [39]. Our own band structure calculations, using the method of Ref. [43], show that the hopping is dominated by paths via the O-p_x-Cu-$d_{(x^2-y^2)}$ and O-p_y-Cu-$d_{(x^2-y^2)}$ conduction band orbitals because the large O^{2-} ions give a noticeable electron density towards the center of the bilayer. This main O-Cu hopping path is directly in the c direction, between equivalent lobes of wave functions on Cu and O, so there is little $\mathbf{k}$ dependence of $t_\perp$, i.e., the *intra*bilayer hopping, and we shall take $t_\perp$ as a constant.

However, the main path for the interbilayer tunneling t_c is via a p_z orbital on the apical oxygen. In a tetragonal cuprate, this would lead, for identical reasons, to the expression that has been claimed for $t_\perp$:

$$t_c = -\frac{t_{c0}}{4}(\cos k_x a - \cos k_y a)^2. \quad (8)$$

This would lead to $t_c = 0$ and again to zero dispersion with k_z on the nodal line, for a tetragonal superconductor, but this result is not exact in orthorhombic YBCO [44] and is not seen in DFT calculations. Nevertheless, the multiple hops for this path and the effects leading to Eq. (8) suggest that t_c will be much smaller than $t_\perp$ near the nodal region, and hence at the crossing points where FS reconstruction can occur. These are the reasons for taking $t_c = 0$ in our modeling.

V. EFFECTS OF THE CDW–FERMI SURFACE CALCULATIONS

We are now in a position to illustrate, by explicit numerical calculations, how various physical effects contribute to the FS reconstruction by the CDWs. In our calculations, we take a double-$\mathbf{q}$ CDW, with incommensurate δ values, which for simplicity we set to $0.32\times 2\pi/a$ for both components, and take δ as independent of field [10,24,25]. We take the value $0.2\times t$ for $t_\perp$. This value is chosen for clarity to give well-separated A and B bands; somewhat smaller values may be needed to fit the experimental QO frequency splittings, and to be consistent with ARPES observations [33] that do not resolve the A-B separation along the nodal direction. For the perturbation due to the CDW, we take $V = 0.15\times t$, giving it a value comparable with the quantity determining the A-B splitting. For the SO interaction, we take a value for α in Eq. (4) of $0.1a\times t$. This was chosen to be sufficiently large to make the SO hybridization gaps easily visible. We have expressed all energy variables in terms of t, so that our calculations of FS areas are independent of the value of t, which then determines the Fermi velocities associated with these areas.

The combination of the CDW δ values and the positions of the unperturbed Fermi surfaces determines the areas of the reconstructed electron pockets. The value of ε_F was chosen to give pocket areas which are close to the 2% of the BZ given by QO measurements. This implies Fermi arcs which are close to the antiferromagnetic BZ boundaries. This is consistent with ARPES observations in underdoped YBCO [33]. Alternatively, the effects of underdoping or PG may reduce the values of t' and t'' below those of Ref. [39]. A reduction by a factor of 2 would give positions of the Fermi arcs

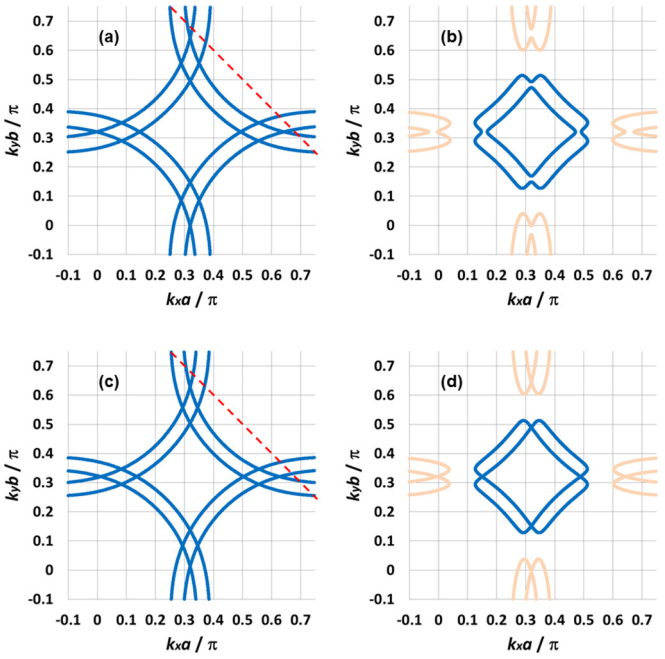

FIG. 2. Reconstructed Fermi surfaces in zero magnetic field created by the CDWs. In (a) are shown the bands in the absence of hybridization by the CDWs. The antiferromagnetic zone boundary is marked by the diagonal red dashed line. In (b) are shown the Fermi surfaces as reconstructed from the Fermi arcs by the CDWs. For both (a) and (b) the SO interaction is nonzero. We assume that the paler parts are removed by the PG. (c) and (d) are calculated with the SO interaction set to zero. By comparison of (b) with (d), one can see which crossings are turned into avoided crossings by the SO interaction. Careful comparison of (a) with (c) shows that the SO interaction also leads to a greater A-B separation, as expected from Eq. (6).

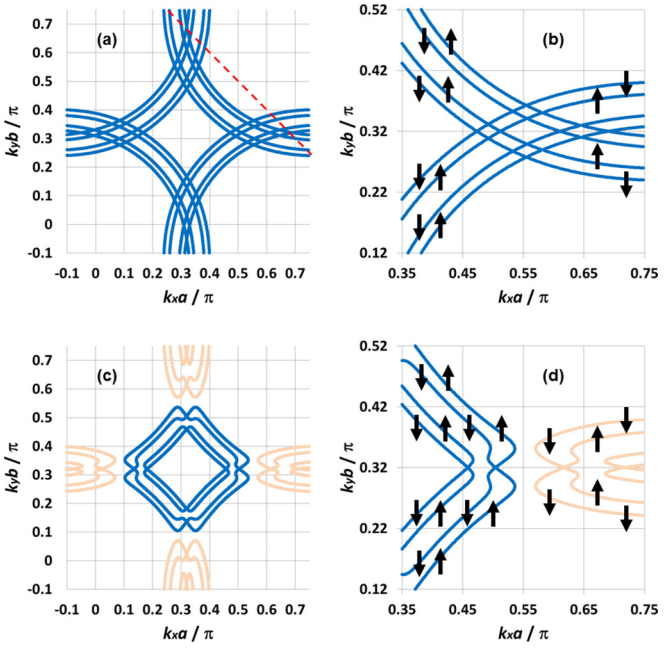

FIG. 3. Reconstructed Fermi surfaces in a magnetic field and details of crossings. (a) The spin-split bands in the absence of hybridization by the CDWs; (b) a close-up of one of the hybridization regions for comparison with (c) and (d). The spin directions in the various bands are marked by arrows. (c),(d) The same regions with the avoided crossings and spin flips caused by the CDW.

in agreement with experiment. A simplistic picture ignoring the PG and constructing an unperturbed FS shape containing $\sim$1.1 holes (doping $p \sim 0.1$) and $\delta \sim 0.32$ would give FS pockets considerably smaller than those observed.

Typical results of numerical diagonalization of the full 16×16 Hamiltonian matrix calculated at zero B_z are shown in Fig. 2. In Figs. 2(a) and 2(c), we give the FS shapes in the absence of the CDW, to make it clear in Figs. 2(b) and 2(d) which states are mixed by the CDWs. In Fig. 2(b), we see a smaller FS sheet that is A in character plus a larger one that is mainly B in character; however, Fig. 2(d) shows that the A-A splitting, which gives the smaller FS in Fig. 2(b), only arises because the SO interaction makes the hybridization effect of the CDW nonzero at the A-A crossings. Without the SO interaction, we would obtain two intersecting Fermi surfaces like those depicted in Figs. 1(e) and 1(f), and these would not give multiple QO frequencies that are observed in experiment.

VI. EFFECTS OF MAGNETIC FIELD AND SO INTERACTIONS ON FERMI SURFACE RECONSTRUCTION

The Zeeman energy of the electron spins at the fields used for QO measurements is substantial. It is comparable to the Landau-level spacing and there are only $\sim$10 Landau levels below the Fermi level in the small electron pockets. In Fig. 3, we show that in addition, the effects of magnetic field along the c direction are nontrivial. Figure 3(a) shows the effects of the Zeeman energy (set to a value $\pm0.1\times t$) on the bands in the absence of hybridization, with an expanded view at a single crossing in Fig. 3(b). The effects of the CDWs are shown in Figs. 3(c) and 3(d). The spin-split Fermi surfaces are labeled with arrows representing the spin directions. Two interesting effects are revealed in Figs. 3(c) and 3(d). It will be noticed that there are places where Fermi surfaces cross each other without any splitting. At the high magnetic fields employed for QO measurements, it is likely that any residual gaps in these regions due to higher-order effects will be ineffective and the electron orbits will tend to pass through them. Another very important qualitative feature of the SO interaction is revealed by tracing the spin directions from regions well away from the crossing region. We find in those places where the SO interaction enables an avoided crossing that the carrier spin direction is flipped as well. As emphasized in Ref. [31], a carrier going around an orbit with spin flip can show an anomalously small average Zeeman energy or g factor. In all the orbits shown in Fig. 3(c), there is an even number of spin flips, so the carriers should have close to zero average Zeeman energy. However, this conclusion is modified if the electron orbits can pass by "magnetic breakdown" through the SO gap or other small gaps. This process can alter both the areas of the orbits and the spin energy, so we now consider it.

VII. MAGNETIC BREAKDOWN

The representation of the motion of a carrier in a lattice in a magnetic field by the progress of its **k** vector around a Fermi surface is an approximation. If the carrier comes to a small "forbidden" region created by an energy gap, it is possible for the particle to "tunnel" through the forbidden region, particularly at high magnetic fields. This is called magnetic breakdown. If two FS sheets approach each other but have a gap between them in **k** space of value k_g, then the probability P of tunneling across the gap is given by [45]

$$P \approx e^{-k_g^2 \ell_m^2}, \tag{9}$$

where ℓ_m is the magnetic length in a field B_z, defined by $\ell_m^2 = \hbar/eB_z$. For the case considered here, the important process is magnetic breakdown from A to A or B to B at the red crossing points in Fig. 1. (We propose that breakdown out of the Fermi arcs towards the edges of the BZ is prevented by the PG.) Assuming that the CDW gaps are comparable with those due to A-B splitting, we may use the QO data to give an order of magnitude for the gap k_g between different FS areas, and this will indicate (independent of our calculations above) at what fields magnetic breakdown may be important. The QO frequencies in YBCO are around 2% of the BZ area, i.e., $\sim 6\times10^{18}$ m^{-2}, and the spread of frequencies is ~40%, giving a gap k_g between the corners of two concentric areas, $\sim 2.5\times10^{8}$ m^{-1}. Now we may write the probability of magnetic breakdown in the form

$$P \approx e^{-B_0/B_z}, \quad \text{where } B_0 = \frac{\hbar k_g^2}{e}. \tag{10}$$

Using our rough estimate of k_g, we obtain $B_0 \sim 40$ T, which is in the range where QO measurements are carried out, and suggests that magnetic breakdown may well be dominant at the highest fields. Indeed, according to our calculations, the hybridization gaps between bands of like character have small SO-induced values at the crossing points. Hence, magnetic breakdown will play an important role even at lower fields, and it will give a high probability that the **k** vectors of the carriers pass straight through these crossings.

VIII. EFFECTS OF TILTING THE MAGNETIC FIELD AWAY FROM THE *c* axis

An important experimental variable in QO measurements is to change the direction of the applied field. In two-dimensional materials, this allows the comparison of the Zeeman and Landau-level spacings, which have a different dependence on angle and can lead to "spin zeros" in the QO signal for particular angles between **B** and the **c** axis [27,46]. There is a further effect of tilting the magnetic field: B_0 in the expression for magnetic breakdown becomes $B_0/\cos(\theta)$ when the field is tilted by an angle θ from **c**, so the probability of magnetic breakdown is decreased. In the present case, there is an additional interest: the SO term in Eq. (4) behaves like a magnetic field in the basal plane, parallel to the unreconstructed Fermi surface and of opposite sign in the two halves of a bilayer. This can interfere with a real magnetic field, which when tilted gives a basal-plane component equal in the two halves of a bilayer.

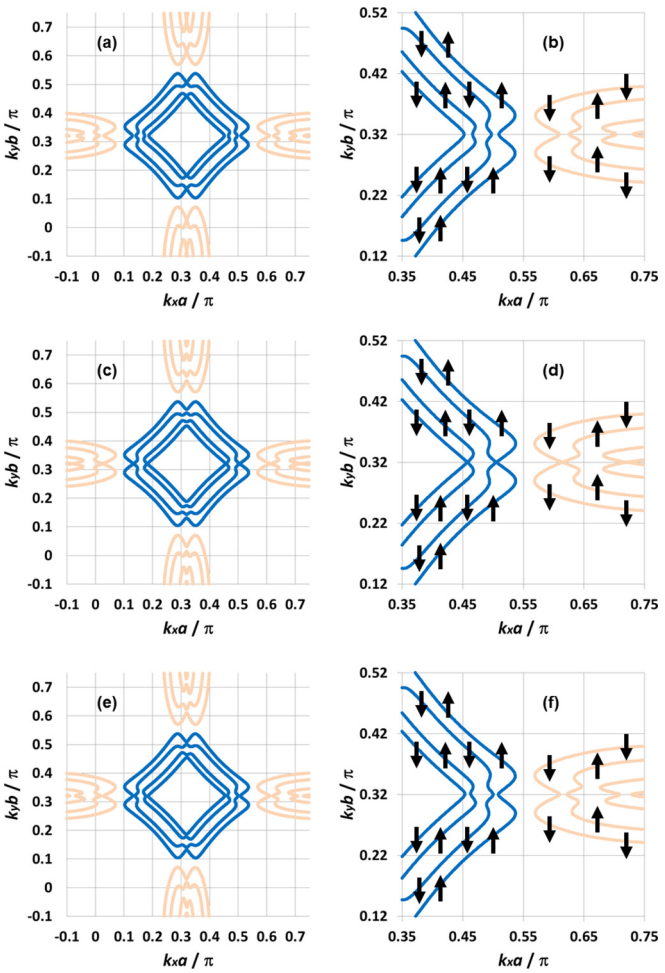

FIG. 4. Effects of tilted magnetic field and SO interaction on Fermi surface reconstruction. (a) The same magnitude of field as in Fig. 3 is applied at an angle of 45° to **c**, tilted towards the y direction. (b) Detail of the removal of spin flips and their replacement by small gaps for the crossings near the k_x direction. (c),(d) are for the field tilted towards **x** and confirm that the SO-induced spin flips are not removed for the crossings close to the field-tilt direction. If the field is tilted towards the xy direction, smaller gaps are created at both crossing points, as indicated in (e) and (f).

In Fig. 4, we show the effect of *field angle* only; we have neglected the weak variation with angle of the electronic g factor (also a SO effect) because it does not give rise to qualitatively new behavior. It will be seen in Figs. 4(a) and 4(b) that a field tilted towards the y direction removes the SO spin flips for the crossings in the k_x direction and replaces them with small gaps, but the spin flips remain for the k_y crossings. This is confirmed by Fig. 4(d), which shows the effect of tilting the field direction towards **x**. When the field is tilted along the xy direction, both SO spin flips are removed and replaced with somewhat smaller gaps, as shown in Figs. 4(e) and 4(f). These gaps arise when the sum of the basal-plane applied field and SO effective field further breaks the bilayer symmetry, so that more CDW hybridization matrix elements become nonzero.

Thus, tilting the magnetic field will introduce a fourfold anisotropy in the values of the gaps and hence in the connectivity of the electron orbits. Our model can therefore

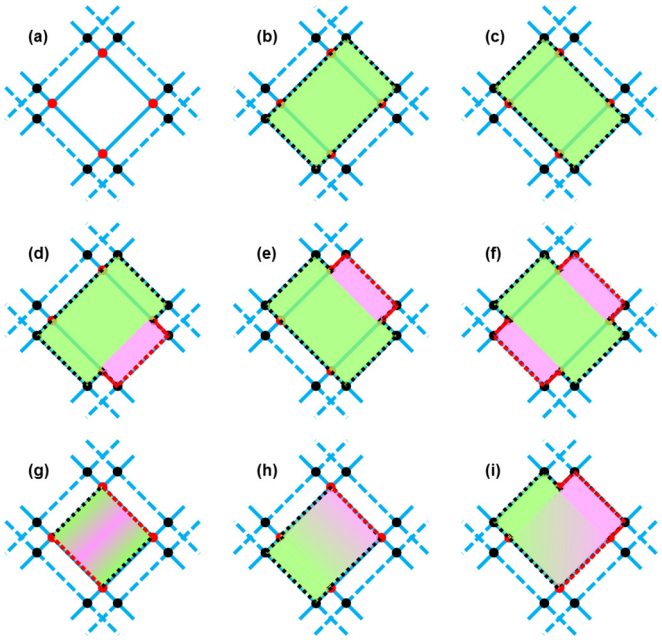

FIG. 5. Fermi surface orbits, magnetic breakdown, and spin-flip. The straight lines in **k** space represent schematically the A and B (dashed) bands that intersect to form the small electron pocket Fermi surfaces. Strong hybridization (which would round the corners) and reflection is expected at the black points marking A-B crossings. Weak hybridization, spin flip on reflection, and a larger probability of transmission is expected at the red A-A crossing points. The shaded areas represent the different kinds of possible **k**-space closed orbits of carriers in a magnetic field which would be detected by QO measurements. The change in color of the orbit from black to red and back represents a flip of the spin of an electron by the SO interaction.

provide a framework for understanding the fourfold variation seen in QO measurements in tilted fields [27]. This depends on the topology of the orbits given by magnetic breakdown, and we now consider this matter in detail.

IX. MAGNETIC BREAKDOWN AND ORBIT AREAS

In Fig. 5, we give a schematic representation of the various **k**-space orbits predicted by this model. The crossings of the A and B (dashed) bands are shown in Fig. 5(a). The black spots on the A-B crossings represent the strong hybridization by the CDWs, which does not lead to electron spin flip. The red spots mark weak hybridization by the CDW in the presence of the SO interaction. If a carrier is reflected by the small gaps at these points, it undergoes a spin flip; if it is transmitted, no spin flip occurs. In Figs. 5(b) and 5(c), the shaded areas are the two orbits of medium area, which would represent the central peak in a typical QO spectrum. This peak is dominant in the experimental data, and is also known to have an electron g factor close to the standard value [27,46]. In our model, these orbits have no spin flips, which agrees with the observed g-factor value. These orbits arise only because of magnetic breakdown, so we deduce that the gaps at the red points are small.

In Figs. 5(d)–5(i), we represent the other possible orbits allowed by the model. In Figs. 5(d) and 5(e) are represented two different orbits of identical area but different orientations; in later panels, we give only the topology, and not all possible orientations. The spin flips are represented by using a black dashed line for paths with one spin orientation and a red one for the other. It will be noted that in orbits shown by Figs. 5(d) to 5(i), there is some cancellation of the electron spin direction. This is a phenomenon pointed out in Ref. [31] and gives a reduced effective g factor as well as less dependence of the orbit area on the value of magnetic field. It is found experimentally that some of the QO sidebands have different spin zero positions from the main frequency. This is an expected consequence of our model. There are, in fact, three orbits, shown by Figs. 5(f), 5(g), and 5(i), which have a g factor close to zero, and Fig. 5(i) has an area similar to Figs. 5(b) and 5(c). When magnetic breakdown is strong, we expect that orbits with many reflections, shown by Figs. 5(f) and 5(g), will have low weight.

These are the predictions of the model for **B** parallel to **c**. As shown earlier, tilting the field away from **c** will not only increase the probability of reflection at some of the red crossing points, it can also replace spin flips with energy gaps at various places, depending on the azimuthal angle of the tilt relative to the **a**, **b** crystal axes. In particular, we find that the orbits shown by Figs. 5(b) and 5(c) acquire additional gaps, which can alter the probability of transmission or change the spin energy on reflection. This and similar effects on the orbits of the type shown by Fig. 5(i), which have the same area, could account for the reported fourfold azimuthal dependence of the QO signal which may arise from these orbits [27]. Our model clearly predicts a wealth of different effects and gives a scenario capable of accounting for the multiple pocket areas given by QO measurements, although a detailed fit of the extensive existing data [2,27,29,30,34,47–57] is beyond the scope of the present paper.

X. DISCUSSION

The model we have described gives a coherent account of the influence of the CDW on the QO spectra observed in underdoped YBCO. We have ignored all effects of the CuO chains, since they appear to be nonmetallic in the underdoped region, and the different orderings of the occupied chains at different dopings appear to have no effect on the smooth variation of QO frequency with doping [57]. We have relied on the pseudogap and underdoping to remove chain and antinodal carrier states which do not appear in QO, Hall, and heat-capacity measurements at high field [34,35], and leave the "Fermi arc" states which are hybridized by the CDWs.

The values of the parameters used in our calculations may be justified as follows. They are all expressed in terms of the nearest-neighbour basal-plane hopping parameter t. A "bare" value of t can be obtained from local density approximation (LDA) calculations and is typically 430 meV (e.g., Ref. [58]). An experimental value of the Fermi velocity can be obtained from the effective mass $m^\star$ and pocket area, both derived from QO data (e.g., Ref. [29]). This allows us to estimate that t is renormalized down to $\sim$100 meV by interactions. The value of $t_\perp$ relative to t is indicated within our model by the observed splitting of the QO pocket areas. The sidebands at $\sim$620 and 440 T show that the linear dimensions of largest and smallest areas differ by $\sim$20%. The value of $t_\perp = 0.2t \sim 20$ meV was

chosen to be slightly larger than the expected experimental value in order to give clear separation of the A and B bands in the figures.

The value of the CDW perturbation V is less obviously indicated by the data; we have chosen a value of $V = 0.15t \sim 15$ meV, which is comparable with $k_B \times$ the onset temperature of CDW order. It is also comparable with the superconducting energy gap, and therefore the CDW and superconductivity will compete. Larger values of V will make the corners of the pockets more rounded and also reduce the average value of the Fermi velocity in the pockets below that given by t.

We propose that magnetic breakdown occurs at the small hybridization gaps arising from the CDW perturbation combined with the SO interaction. If we suppose that the breakdown field B_0 is similar to the value 2.7 T used in a fitting of a rather different model [27], then we may use Eq. (10) to estimate the gap k_g due to this hybridization and obtain $\sim$0.4% of the width of the Brillouin zone. In our calculations, we find that k_g is proportional both to V and δ_{SO} and estimate that the expected k_g would arise from a value of $\alpha \sim 0.05a \times t \sim 5a$ meV Å. We used twice this value in our calculations in order to make the SO hybridization gaps clearly visible in the figures.

The spin-orbit interaction has another effect on the results: it favors spin orientations in the basal plane [see Eq. (4)], so it can reduce the g factor for the electron spins when the **B** field is applied parallel to **c**. For a Zeeman splitting that is small compared with $t_\perp$, we find that the size of the effect on g is determined by $\delta_{SO}/t_\perp$ and not by $\delta_{SO}/\mu B_z$. For small δ_{SO}, the fractional change in g is given by $1/2(\delta_{SO}/t_\perp)^2$. Our value of $\alpha \sim 0.05a \times t$ gives $\sim$4 % reduction in g. Hence, $g \sim 2$ and the Zeeman splitting due to a c-axis magnetic field may be calculated. We used a rather large value in our calculations: $\mu B = 0.1t \sim 10$ meV, which corresponds to a field of more than 150 T. This was chosen to make the physical effects of the magnetic field and the spin flips clear in the figures.

Recent QO measurements [30] have suggested the existence of an additional holelike area, approximately 1/5 of those discussed here, and it was proposed [59] that the pseudogap can also explain this result, which does not come out of our calculations. However, it seems likely that these experimental results arise either from mixing of QO frequencies, which can arise in two-dimensional materials from chemical potential oscillations [54] or "Stark interference" [60] corresponding to effects on transport properties of the difference between two areas traversed by electrons [31].

A notable feature of the CDW state in YBCO—and in other materials—is that the **q** vector of the CDW appears not to be a nesting vector between two parallel sheets of Fermi surface. It is clear that the nesting argument, which is persuasive in one dimension (1D) does not necessarily apply in 2D and 3D [61,62]. The question still remains: What is the driving force for the CDW and what determines its **q** vectors?

The picture we have of FS reconstruction in YBCO should also be tested against the field dependence of the Hall effect [3,63]. It has been pointed out [64] that the positive and negative curvatures of the reconstructed pockets give rise to a field dependence of the Hall effect, with a large value and electronlike sign at high fields. The *magnitude* of the high-field Hall coefficient is simply related to the number of carriers, and two pockets each occupying $\sim$2% of the BZ would give a value ~ -14 mm^3/C. Earlier data [3] gave a value much larger than this, corresponding more closely to a single-electron pocket rather than the two we obtain from calculation. However, more recent data from the same group [63] is in good agreement with expectations.

We have used ARPES measurements to indicate those portions of the Fermi surface which remain after the effects of the pseudogap and therefore can be reconstructed by the CDW. However, although CDWs exist in zero magnetic field, there have been no reports of a reconstructed FS observed by ARPES. QO measurements are a bulk effect, and it is possible that the immediate surface—to which ARPES is sensitive—does not support a strong enough CDW. It is also possible that the pocket signal is too weak in ARPES or would only appear at high fields where QO measurements are performed and ARPES measurements are impossible.

XI. CONCLUSIONS

In conclusion, we have demonstrated how multiple QO frequencies observed in YBCO are naturally explained by the odd symmetry of the CDW order, combined with the effects of spin-orbit interaction and magnetic breakdown. Our minimal model for a single bilayer gives an account of the main features expected for the reconstructed part of the Fermi surface in underdoped YBCO and leads to a rich phenomenology. Our calculations have been carried out for reasonable values of the parameters to illustrate the effects that are produced in the published quantum oscillation data, including the fourfold anisotropy present when the field is tilted away from the c axis. It is interesting that the tilted field not only probes the electronic structure which was present with field perpendicular to the bilayers, but also modifies it. It remains for detailed fits, (which will need to include the effects of magnetic breakdown, giving a field dependence to the amplitudes of the various QO frequencies), to establish whether the role of the CDW in Fermi surface reconstruction in YBCO can be fully established.

ACKNOWLEDGMENTS

We acknowledge the UK EPSRC for funding under Grants No. EP/J016977/1 and No. EP/J015423/1, and helpful discussions with Mike Gunn, Suchitra Sebastian, and Tim Ziman. The work in Greece was partially supported by the European Union's Seventh Framework Program (FP7-REGPOT-2012-2013-1) under Grant Agreement No. 316165.

[1] B. Vignolle, A. Carrington, R. A. Cooper, M. M. J. French, A. P. Mackenzie, C. Jaudet, D. Vignolles, and C. Proust, Nature (London) **455**, 952 (2008).

[2] N. Doiron-Leyraud, C. Proust, D. LeBoeuf, J. Levallois, J.-B. Bonnemaison, R. Liang, D. A. Bonn, W. N. Hardy, and L. Taillefer, Nature (London) **447**, 565 (2007).

[3] D. LeBoeuf, N. Doiron-Leyraud, J. Levallois, R. Daou, J.-B. Bonnemaison, N. E. Hussey, L. Balicas, B. J. Ramshaw, R. Liang, D. A. Bonn, W. N. Hardy, S. Adachi, C. Proust, and L. Taillefer, Nature (London) **450**, 533 (2007).

[4] J. Chang, R. Daou, Cyril Proust, David LeBoeuf, Nicolas Doiron-Leyraud, Francis Laliberté, B. Pingault, B. J. Ramshaw, Ruixing Liang, D. A. Bonn, W. N. Hardy, H. Takagi, A. B. Antunes, I. Sheikin, K. Behnia, and Louis Taillefer, Phys. Rev. Lett. **104**, 057005 (2010).

[5] T. Wu, H. Mayaffre, S. Kramer, M. Horvatic, C. Berthier, W. N. Hardy, R. Liang, D. A. Bonn, and M.-H. Julien, Nature (London) **477**, 191 (2011).

[6] G. Ghiringhelli, M. Le Tacon, M. Minola, S. Blanco-Canosa, C. Mazzoli, N. B. Brookes, G. M. De Luca, A. Frano, D. G. Hawthorn, F. He, T. Loew, M. M. Sala, D. C. Peets, M. Salluzzo, E. Schierle, R. Sutarto, G. A. Sawatzky, E. Weschke, B. Keimer, and L. Braicovich, Science **337**, 821 (2012).

[7] A. J. Achkar, R. Sutarto, X. Mao, F. He, A. Frano, S. Blanco-Canosa, M. Le Tacon, G. Ghiringhelli, L. Braicovich, M. Minola, M. Moretti Sala, C. Mazzoli, Ruixing Liang, D. A. Bonn, W. N. Hardy, B. Keimer, G. A. Sawatzky, and D. G. Hawthorn, Phys. Rev. Lett. **109**, 167001 (2012).

[8] S. Blanco-Canosa, A. Frano, T. Loew, Y. Lu, J. Porras, G. Ghiringhelli, M. Minola, C. Mazzoli, L. Braicovich, E. Schierle, E. Weschke, M. Le Tacon, and B. Keimer, Phys. Rev. Lett. **110**, 187001 (2013).

[9] S. Blanco-Canosa, A. Frano, E. Schierle, J. Porras, T. Loew, M. Minola, M. Bluschke, E. Weschke, B. Keimer, and M. Le Tacon, Phys. Rev. B **90**, 054513 (2014).

[10] J. Chang, E. Blackburn, A. T. Holmes, N. B. Christensen, J. Larsen, J. Mesot, R. Liang, D. A. Bonn, W. N. Hardy, A. Watenphul, M. v. Zimmermann, E. M. Forgan, and S. M. Hayden, Nat. Phys. **8**, 871 (2012).

[11] E. Blackburn, J. Chang, M. Hucker, A. T. Holmes, N. B. Christensen, R. Liang, D. A. Bonn, W. N. Hardy, U. Rütt, O. Gutowski, M. v. Zimmermann, E. M. Forgan, and S. M. Hayden, Phys. Rev. Lett. **110**, 137004 (2013).

[12] M. Hücker, N. B. Christensen, A. T. Holmes, E. Blackburn, E. M. Forgan, R. Liang, D. A. Bonn, W. N. Hardy, O. Gutowski, M. v. Zimmermann, S. M. Hayden, and J. Chang, Phys. Rev. B **90**, 054514 (2014).

[13] R. Comin, A. Frano, M. M. Yee, Y. Yoshida, H. Eisaki, E. Schierle, E. Weschke, R. Sutarto, F. He, A. Soumyanarayanan, Y. He, M. Le Tacon, I. S. Elfimov, J. E. Hoffman, G. A. Sawatzky, B. Keimer, and A. Damascelli, Science **343**, 390 (2014).

[14] E. H. da Silva Neto, P. Aynajian, A. Frano, R. Comin, E. Schierle, E. Weschke, A. Gyenis, J. Wen, J. Schneeloch, Z. Xu, S. Ono, G. Gu, M. Le Tacon, and A. Yazdani, Science **343**, 393 (2014).

[15] M. Hashimoto, G. Ghiringhelli, W.-S. Lee, G. Dellea, A. Amorese, C. Mazzoli, K. Kummer, N. B. Brookes, B. Moritz, Y. Yoshida, H. Eisaki, Z. Hussain, T. P. Devereaux, Z.-X. Shen, and L. Braicovich, Phys. Rev. B **89**, 220511 (2014).

[16] V. Thampy, M. P. M. Dean, N. B. Christensen, L. Steinke, Z. Islam, M. Oda, M. Ido, N. Momono, S. B. Wilkins, and J. P. Hill, Phys. Rev. B **90**, 100510 (2014).

[17] W. Tabis, Y. Li, M. L. Tacon, L. Braicovich, A. Kreyssig, M. Minola, G. Dellea, E. Weschke, M. J. Veit, M. Ramazanoglu, A. I. Goldman, T. Schmitt, G. Ghiringhelli, N. Barisic, M. K. Chan, C. J. Dorow, G. Yu, X. Zhao, B. Keimer, and M. Greven, Nat. Commun. **5**, 5875 (2014).

[18] N. B. Christensen, J. Chang, J. Larsen, M. Fujita, M. Oda, M. Ido, N. Momono, E. M. Forgan, A. T. Holmes, J. Mesot, M. Huecker, and M. v. Zimmermann, arXiv:1404.3192.

[19] T. P. Croft, C. Lester, M. S. Senn, A. Bombardi, and S. M. Hayden, Phys. Rev. B **89**, 224513 (2014).

[20] R. Comin, R. Sutarto, F. He, E. H. da Silva Neto, L. Chauviere, A. Fraño, R. Liang, W. N. Hardy, D. A. Bonn, Y. Yoshida, H. Eisaki, A. J. Achkar, D. G. Hawthorn, B. Keimer, G. A. Sawatzky, and A. Damascelli, Nat. Mater. **14**, 796 (2015).

[21] K. Fujita, C. K. Kim, I. Lee, J. Lee, M. H. Hamidian, I. A. Firmo, S. Mukhopadhyay, H. Eisaki, S. Uchida, M. J. Lawler, E.-A. Kim, and J. C. Davis, Science **344**, 612 (2014).

[22] E. H. da Silva Neto, R. Comin, F. He, R. Sutarto, Y. Jiang, R. L. Greene, G. A. Sawatzky, and A. Damascelli, Science **347**, 282 (2015).

[23] E. M. Forgan, E. Blackburn, A. T. Holmes, A. K. R. Briffa, J. Chang, L. Bouchenoire, S. D. Brown, Ruixing Liang, D. Bonn, W. N. Hardy, N. B. Christensen, M. V. Zimmermann, M. Hücker, and S. M. Hayden, Nat. Commun. **6**, 10064 (2015).

[24] S. Gerber, H. Jang, H. Nojiri, S. Matsuzawa, H. Yasumura, D. A. Bonn, R. Liang, W. N. Hardy, Z. Islam, A. Mehta, S. Song, M. Sikorski, D. Stefanescu, Y. Feng, S. A. Kivelson, T. P. Devereaux, Z.-X. Shen, C.-C. Kao, W.-S. Lee, D. Zhu, and J.-S. Lee, Science **350**, 949 (2015).

[25] J. Chang, E. Blackburn, O. Ivashko, A. T. Holmes, N. B. Christensen, M. Hücker, Ruixing Liang, D. A. Bonn, W. N. Hardy, U. Rütt, M. v. Zimmermann, E. M. Forgan, and S. M. Hayden, arXiv:1511.06092.

[26] D. LeBoeuf, S. Kramer, W. N. Hardy, R. Liang, D. A. Bonn, and C. Proust, Nat. Phys. **9**, 79 (2013).

[27] S. E. Sebastian and N. Harrison, Nature (London) **511**, 61 (2014).

[28] N. Harrison and S. E. Sebastian, New J. Phys. **14**, 095023 (2012).

[29] S. E. Sebastian, N. Harrison, and G. G. Lonzarich, Rep. Prog. Phys. **75**, 102501 (2012).

[30] N. Doiron-Leyraud, S. Badoux, S. Rene de Cotret, S. Lepault, D. LeBoeuf, F. Laliberte, E. Hassinger, B. J. Ramshaw, D. A. Bonn, W. N. Hardy, R. Liang, J.-H. Park, D. Vignolles, B. Vignolle, L. Taillefer, and C. Proust, Nat. Commun. **6**, 6034 (2015).

[31] N. Harrison, B. J. Ramshaw, and A. Shekhter, Sci. Rep. **5**, 10914 (2015).

[32] A. V. Maharaj, Y. Zhang, B. J. Ramshaw, and S. A. Kivelson, Phys. Rev. B **93**, 094503 (2016).

[33] D. Fournier, G. Levy, Y. Pennec, J. L. McChesney, A. Bostwick, E. Rotenberg, R. Liang, W. N. Hardy, D. A. Bonn, I. S. Elfimov, and A. Damascelli, Nat. Phys. **6**, 905 (2010).

[34] S. C. Riggs, O. Vafek, J. B. Kemper, J. B. Betts, A. Migliori, F. F. Balakirev, W. N. Hardy, R. Liang, D. A. Bonn, and G. S. Boebinger, Nat. Phys. **7**, 332 (2011).

[35] C. Marcenat, A. Demuer, K. Beauvois, B. Michon, A. Grockowiak, R. Liang, W. Hardy, D. A. Bonn, and T. Klein, Nat. Commun. **6**, 7927 (2015).

[36] A. K. R. Briffa, E. Blackburn, S. M. Hayden, E. A. Yelland, M. W. Long, and E. M. Forgan (unpublished).

[37] B. Vignolle, B. J. Ramshaw, J. Day, D. LeBoeuf, S. Lepault, R. Liang, W. N. Hardy, D. A. Bonn, L. Taillefer, and C. Proust, Phys. Rev. B **85**, 224524 (2012).

[38] Y. A. Bychkov and E. I. Rashba, J. Phys. C **17**, 6039 (1984).

[39] O. K. Andersen, A. I. Liechtenstein, O. Jepsen, and E Paulsen, J. Phys. Chem. Solids **56**, 1573 (1995).

[40] D. Garcia-Aldea and S. Chakravarty, New J. Phys. **12**, 105005 (2010).
[41] I. S. Elfimov, G. A. Sawatzky, and A. Damascelli, Phys. Rev. B **77**, 060504(R) (2008).
[42] A. Carrington and E. A. Yelland, Phys. Rev. B **76**, 140508(R) (2007).
[43] P. Blaha, K. Schwarz, G. K. H. Madsen, D. Kvasnicka, and J. Luitz, *WIEN2k: An Augmented Plane Wave Plus Local Orbitals Program for Calculating Crystal Properties* (Karlheinz Schwarz, Techn. Universität Wien, Austria, 2001).
[44] T. Xiang and J. M. Wheatley, Phys. Rev. Lett. **77**, 4632 (1996).
[45] J.-Y. Fortin, J. Bellissard, M. Gusmao, and T. Ziman, Phys. Rev. B **57**, 1484 (1998).
[46] B. J. Ramshaw, Baptiste Vignolle, James Day, Ruixing Liang, W. N. Hardy, Cyril Proust, and D. A. Bonn, Nat. Phys. **7**, 234 (2011).
[47] S. E. Sebastian, N. Harrison, E. Palm, T. P. Murphy, C. H. Mielke, R. Liang, D. A. Bonn, W. N. Hardy, and G. G. Lonzarich, Nature (London) **454**, 200 (2008).
[48] A. F. Bangura, J. D. Fletcher, A. Carrington, J. Levallois, M. Nardone, B. Vignolle, P. J. Heard, N. Doiron-Leyraud, D. LeBoeuf, L. Taillefer, S. Adachi, C. Proust, and N. E. Hussey, Phys. Rev. Lett. **100**, 047004 (2008).
[49] E. A. Yelland, J. Singleton, C. H. Mielke, N. Harrison, F. F. Balakirev, B. Dabrowski, and J. R. Cooper, Phys. Rev. Lett. **100**, 047003 (2008).
[50] A. Audouard, C. Jaudet, D. Vignolles, R. Liang, D. A. Bonn, W. N. Hardy, L. Taillefer, and C. Proust, Phys. Rev. Lett. **103**, 157003 (2009).
[51] S. E. Sebastian, N. Harrison, M. M. Altarawneh, C. H. Mielke, R. Liang, D. A. Bonn, W. N. Hardy, and G. G. Lonzarich, Proc. Natl. Acad. Sci. USA **107**, 6175 (2010).
[52] S. E. Sebastian, N. Harrison, M. M. Altarawneh, R. Liang, D. A. Bonn, W. N. Hardy, and G. G. Lonzarich, Phys. Rev. B **81**, 140505(R) (2010).
[53] S. E. Sebastian, N. Harrison, P. A. Goddard, M. M. Altarawneh, C. H. Mielke, R. Liang, D. A. Bonn, W. N. Hardy, O. K Andersen, and G. G. Lonzarich, Phys. Rev. B **81**, 214524 (2010).
[54] J. Singleton, C. de la Cruz, R. D. McDonald, S. Li, M. M. Altarawneh, P. Goddard, I. Franke, D. Rickel, C. H. Mielke, X. Yao, and P. Dai, Phys. Rev. Lett. **104**, 086403 (2010).
[55] S. E. Sebastian, N. Harrison, M. M. Altarawneh, R. Liang, D. A. Bonn, W. N. Hardy, and G. G. Lonzarich, Nat. Commun. **2**, 471 (2011).
[56] S. E. Sebastian, N. Harrison, R. Liang, D. A. Bonn, W. N. Hardy, C. H. Mielke, and G. G. Lonzarich, Phys. Rev. Lett. **108**, 196403 (2012).
[57] B. Vignolle, D. Vignolles, M.-H. Julien, and C. Proust, C. R. Phys. **12**, 446 (2011).
[58] E. Pavarini, I. Dasgupta, T. Saha-Dasgupta, O. Jepsen, and O. K. Andersen, Phys. Rev. Lett. **87**, 047003 (2001)
[59] A. Allais, D. Chowdhury, and S. Sachdev, Nat. Commun. **5**, 5771 (2014).
[60] R. W. Stark and C. B. Friedberg, Phys. Rev. Lett. **26**, 556 (1971).
[61] M. D. Johannes and I. I. Mazin, Phys. Rev. B **77**, 165135 (2008).
[62] X. Zhu, Y. Cao, J. Zhang, E. W. Plummer, and J. Guo, Proc. Natl. Acad. Sci. USA **112**, 2367 (2015).
[63] G. Grissonnanche, F. Laliberte, S. Dufour-Beausejour, M. Matusiak, S. Badoux, F. F. Tafti, B. Michon, A. Riopel, O. Cyr-Choiniere, J. C. Baglo, B. J. Ramshaw, R. Liang, D. A. Bonn, W. N. Hardy, S. Kramer, D. LeBoeuf, D. Graf, N. Doiron-Leyraud, and L. Taillefer, Phys. Rev. B **93**, 064513 (2016).
[64] N. Harrison and S. E. Sebastian, arXiv:1502.02273.